Characterization and X-ray Absorption Spectroscopic Studies of Bis[quinato(2−)]oxochromate(V)[1]

Rachel Codd, Aviva Levina, Lianbo Zhang, Trevor W. Hambley, and Peter A. Lay*

School of Chemistry, University of Sydney, Sydney 2006, NSW, Australia

Received June 22, 1999

A new Cr(V) complex, $K[Cr^{V}O(qaH_3)_2]\cdot H_2O$ (**Ia**; qaH_3 = quinato = (1*R*,3*R*,4*R*,5*R*)-1,3,4,5-tetrahydroxycyclohexanecarboxylato(2−)), synthesized by the reaction of $K_2Cr_2O_7$ with excess qaH_5 in MeOH (Codd, R.; Lay, P. A. *J. Am. Chem. Soc.* **1999**, *121*, 7864−7876), has been characterized by microanalyses, electrospray mass spectra, and UV−visible, CD, IR, EPR, and X-ray absorption spectroscopies. This complex is of interest because of its ability to act as both a structural and a biomimetic model for a range of Cr(V) species believed to be generated in vivo during the intracellular reduction of carcinogenic Cr(VI). The Na^+ analogue of **Ia** (**Ib**) has also been isolated and characterized by microanalyses and IR and X-ray absorption spectroscopies. The reaction of Cr(VI) with MeOH in the presence of qaH_5 that leads to **I** proceeds via a Cr(IV) intermediate (observed by UV−visible spectroscopy), and a mechanism for the formation of **I** has been proposed. DMF or DMSO solutions of **I** are stable for several days at 25 °C, while **I** in aqueous solution (pH = 4) disproportionates to Cr(VI) and Cr(III) in minutes. The likely structures in the solid state for **Ia** (14 K) and **Ib** (∼293 K) have been determined using both single-scattering (**Ia,b**) and multiple-scattering (**Ia**) analyses of XAFS data. These analyses have shown the following: (i) In agreement with the results from the other spectroscopic techniques, the quinato ligands are bound to Cr(V) by 2-hydroxycarboxylato moieties, with Cr−O bond lengths of 1.55, 1.82, and 1.94 Å for the oxo, alcoholato, and carboxylato O atoms, respectively. (ii) The position of an oxo O atom is somewhat disordered. This is consistent with molecular mechanics modeling of the likely structures. The XAFS, EPR, and IR spectroscopic evidence points to the existence of hydrogen bonds between the oxo ligand and the 3,4,5-OH groups of the quinato ligands in the solid state of **I**.

Introduction

Current interest in Cr(V) complexes[2,3] has focused mainly on revealing their potential roles as reactive intermediates in Cr-induced carcinogenesis.[4,5] According to Wetterhahn's uptake-reduction model,[6] chromate(VI) ions enter cells through the anion channels and undergo reduction by intracellular components, ultimately leading to Cr(III) complexes. However, intermediates of this reduction, such as Cr(V), Cr(IV), and organic radicals, are stronger oxidants than Cr(VI) itself and are able to cause substantial alterations to the genetic apparatus of the cell. For instance, well-characterized Cr(V/IV) complexes cause in vitro DNA cleavage (under the conditions where the generation of reactive oxygen species is excluded)[7−12] and cause mutations in bacterial and mammalian cells.[7,8,12,13] On the other hand, generation of relatively stable Cr(V) species in cellular organelles, whole cells, and living animals, treated with Cr(VI), has been shown by EPR spectroscopy.[14−19]

Various types of ligands are thought to participate in the stabilization of Cr(V/IV) in cellular media. Uptake and reduction

(1) Abbreviations: $ehbaH_2$ = 2-ethyl-2-hydroxybutanoic acid; $hmbaH_2$ = 2-hydroxy-2-methylbutanoic acid; qaH_5 = quinic acid = (1*R*,3*R*,-4*R*,5*R*)-1,3,4,5-tetrahydroxycyclohexanecarboxylic acid; ESMS = electrospray mass spectroscopy; FT = Fourier transform; MM = molecular mechanics; MS = multiple scattering; SS = single scattering; XAFS = X-ray absorption fine structure; XANES = X-ray absorption near-edge structure.

(2) Farrell, R. P.; Lay, P. A. *Comments Inorg. Chem.* **1992**, *13*, 133−175 and references therein.
(3) Barr-David, G.; Charara, M.; Codd, R.; Farrell, R. P.; Irwin, J. A.; Lay, P. A.; Bramley, R.; Brumby, S.; Ji, J.-Y.; Hanson, G. R. *J. Chem. Soc., Faraday Trans.* **1995**, *91*, 1207−1216 and references therein.
(4) *IARC. Monographs on the Evaluation of the Carcinogenic Risk of Chemicals to Humans. Vol. 49. Chromium, Nickel and Welding;* International Agency on the Research of Cancer: Lyon, France, 1990.
(5) For the recent review of the studies of Cr carcinogenicity, see: (a) Costa, M. *Crit. Rev. Toxicol.* **1997**, *27*, 431−442. (b) Singh, J.; Carlisle, D. L.; Pritchard, D. E.; Patierno, S. R. *Oncol. Rep.* **1998**, *5*, 1307−1318 and references therein.
(6) Connett, P.; Wetterhahn, K. E. *Struct. Bonding (Berlin)* **1983**, *54*, 93−124.
(7) Farrell, R. P.; Judd, R. J.; Lay, P. A.; Dixon, N. E.; Baker, R. S. U.; Bonin, A. M. *Chem. Res. Toxicol.* **1989**, *2*, 227−229.
(8) Barr-David, G.; Hambley, T. W.; Irwin, J. A.; Judd, R. J.; Lay, P. A.; Martin, B. M.; Bramley, R.; Dixon, N. E.; Hendry, P.; Ji, J.-Y.; Baker, R. S. U.; Bonin, A. M. *Inorg. Chem.* **1992**, *31*, 4906−4908.
(9) Sugden, K. D.; Wetterhahn, K. E. *Chem. Res. Toxicol.* **1997**, *10*, 1397−1406.
(10) Bose, R. N.; Fonkeng, B. S.; Moghaddas, S.; Stroup, D. *Nucleic Acids Res.* **1998**, *26*, 1588−1596.
(11) Levina, A.; Barr-David, G.; Codd, R.; Lay, P. A.; Dixon, N. E.; Hammershøi, A.; Hendry, P. *Chem. Res. Toxicol.* **1999**, *12*, 371−381.
(12) Dillon, C. T.; Lay, P. A.; Bonin, A. M.; Dixon, N. E.; Collins, T. J.; Kostka, K. L. *Carcinogenesis* **1993**, *14*, 1875−1880.
(13) Dillon, C. T.; Lay, P. A.; Bonin, A. M.; Cholewa, M.; Legge, G. J. F.; Collins, T. J.; Kostka, K. L. *Chem. Res. Toxicol.* **1998**, *11*, 119−129.
(14) Jennette, K. W. *J. Am. Chem. Soc.* **1982**, *104*, 874−875.
(15) Ross, S. C.; Gorman, N.; Wetterhahn, K. E. *Chem. Res. Toxicol.* **1988**, *1*, 101−107.
(16) Liebross, R. H.; Wetterhahn, K. E. *Carcinogenesis* **1992**, *13*, 2113−2120.
(17) Shi, X.; Dalal, N. S.; Vallyathan, V. *Arch. Biochem. Biophys.* **1991**, *290*, 381−386.
(18) Liu, K. J.; Shi, X.; Jiang, J.; Goda, F.; Dalal, N.; Swartz, H. M. *Ann. Clin. Lab. Sci.* **1996**, *26*, 176−184.
(19) Liu, K. J.; Mäder, K.; Shi, X.; Swartz, H. M. *Magn. Res. Med.* **1997**, *38*, 524−526.

10.1021/ic990730b CCC: $19.00
Published on Web 02/15/2000

of insoluble Cr(VI) particles by phagocytosis take place in lysosomes at pH = 4−5.[20,21] These conditions favor the formation of Cr(V/IV) 2-hydroxycarboxylato complexes (as well as of Cr(IV) 1,2-dicarboxylato complexes).[22] Under normal physiological pH conditions (pH ∼ 7.4), Cr(V) (but not Cr(IV)) is probably stabilized by the complexation with 1,2-diolato moieties of carbohydrates.[22−24] Thus, the pH dependence of the formation of Cr(V) complexes with different ligand types is likely to be important with respect to their biological activities.

The relatively stable 2-hydroxycarboxylato complex, Na[$Cr^{V}O(ehba)_2$],[25,26] is by far the most popular model compound used in the studies of Cr(V) biological activity.[7−11] However, a deeper understanding of Cr(V) roles in Cr-induced carcinogenesis requires the use of more biologically relevant models, possessing the following: (i) the possibility of 1,2-diolato coordination; (ii) chirality; (iii) the ability to form inter- and intramolecular hydrogen bonds. Many Cr(V) intermediates, formed in the reactions of Cr(VI) with biological reductants in solutions, have been observed by EPR spectroscopy,[3,23,24,27−30] but none of them has been isolated and fully characterized.[31]

A naturally occurring ligand, quinic acid (qaH_5),[32] is likely to be well suited for stabilization of Cr(V), since it contains a

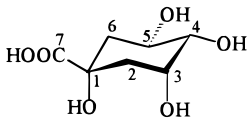

qaH$_5$

tertiary 2-hydroxycarboxylato group, similar to those of the well-known Cr(V) stabilizing ligands, $ehbaH_2$ and $hmbaH_2$.[2,25] On the other hand, the hydroxy-substituted cyclohexane ring and chirality of qaH_5 resemble carbohydrates and its multifunctional nature explains its tendency to form polynuclear complexes with transition metal ions, such as Cu(II)[33] and V(IV/V).[34]

Many studies on Cr(V) complexes have been performed by EPR spectroscopy,[3,23,24,27] and empirical correlations have been developed to predict the coordination environment of Cr(V) from the g_{iso} and A_{iso} values.[3] However, more extensive information about the structures of metal complexes can be obtained from the analysis of XAFS spectra.[35] While the nature of donor atoms in the first coordination shell and the metal−ligand bond lengths are determined by single-scattering (SS) analysis of XAFS spectra, application of a multiple-scattering (MS) method allows the following: (i) improved resolution of similar bond lengths; (ii) detailed studies of second and more distant coordination shells; (iii) the determination of the bond angles.[36,37]

Recently, we reported the synthesis of a new relatively stable Cr(V) complex, K[$Cr^{V}O(qa)_2$]·H_2O (**Ia**), and EPR spectroscopic studies of its speciation in aqueous solutions.[23] In the current work, **Ia** and its Na^+ analogue **Ib** have been characterized by a range of spectroscopic techniques and their likely structures in the solid state have been determined from XAFS, EPR, and IR spectroscopies.

Experimental Section

Caution! Cr(VI) compounds are human carcinogens,[4,5] and the Cr(V) complexes are mutagenic, rapidly cleave DNA at micromolar concentrations, and are potential carcinogens.[7−13] Appropriate precautions should be taken to avoid skin contact and inhalation of Cr(VI) and Cr(V) solutions and dusts.

Reagents. The following reagents of analytical grade were used without purification: qaH_5 (ICN Biomedicals), $K_2Cr_2O_7$, $Na_2Cr_2O_7$·$2H_2O$, NaCl, KCl, KBr, and $(NH_4)_2Fe(SO_4)_2$·$6H_2O$ (all Merck); $ehbaH_2$, diethyl ether, 2-propanol, *tert*-butyl alcohol, and BN (all Aldrich). Aldrich HPLC grade solvents: methanol, ethanol, acetone, DMF, and DMSO were used without purification. Water was purified by the Milli-Q method.

Synthesis of the Cr(V) complexes. K[$Cr^{V}O(qaH_3)_2$]·H_2O (**Ia**) was synthesized by the reaction of $K_2Cr_2O_7$ with excess qaH_5 in methanol, as described previously.[23] Anal. Calcd for $C_{14}H_{22}O_{14}CrK$: C, 33.27; H, 4.39; Cr, 10.29; K, 7.74. Found: C, 33.11; H, 4.10; Cr, 10.60; K, 7.31. ESMS (DMF): m/z = 448.7 (charge 1−). FTIR (KBr matrix): 3300 (s, br), 2950 (w), 1684 (s), 1677 (s), 1444 (w), 1419 (w), 1336 (w), 1288 (m), 1263 (m), 1241 (m), 1157 (w), 1118 (m), 1070 (m), 1050 (m), 1050 (m), 993 (s), 962 (w), 846 (w), 824 (m), 752 (w), 696 (m), 638 (m), 574 (w), 532 (w), 463 (m) cm^{-1}. EPR (solid): g = 1.979. Spectral data for **Ia** in solutions are summarized in Table 1. Despite repeated attempts, no crystals of **Ia** suitable for X-ray crystallography have been obtained as yet. The analogous synthesis using $Na_2Cr_2O_7$·$2H_2O$ instead of $K_2Cr_2O_7$ produced a very hygroscopic red-brown powder, assigned as Na[$Cr^{V}O(qaH_3)_2$]·$2H_2O$·X (**Ib**), where X = $C_6H_6O_4$ is the ligand oxidation product (yield 48%). Anal. Calcd for $C_{20}H_{30}O_{19}CrNa$: C, 36.99; H, 4.66; Cr, 8.01; Na, 3.54. Found: C, 36.51; H, 4.89; Cr, 8.07; Na, 3.09. FTIR (KBr matrix): 3358 (s, br), 2927 (w), 1696 (s), 1684 (s), 1653 (s), 1647 (s), 1636 (s), 1560 (w), 1338 (m,br), 1151 (w), 1115 (m), 1067 (s), 995 (s), 965 (w), 914 (w), 889 (w), 821 (s), 757 (m), 690 (m), 618 (s), 536 (m) cm^{-1}. UV−vis (DMSO): λ, nm (ϵ, M^{-1} cm^{-1}) 542 (252). Na[$Cr^{V}O(ehba)_2$]·H_2O (**II**) was synthesized according to the method of Krumpolc and Roček,[25] and its purity was confirmed by microanalysis and IR and UV−visible spectroscopies.

Physical Measurements. Microanalyses (C, H, and Cr) were performed by the Australian National University Microanalytical Service. Analyses for Na and K were performed on a Corning 400 flame photometer using NaCl or KCl as calibration stardards. The ESMS analyses were performed using a Finnigan LSQ mass spectrometer under the following conditions: spray voltage 5 kV, sheath gas (N_2) pressure 60 psi, mobile phase MeOH/H_2O (1:1 v/v) at 0.2 mL

(20) Elias, Z.; Poirot, O.; Pezerat, H.; Suquet, H.; Schneider, O.; Danière, M. C.; Terzetti, F.; Baruthio, F.; Fournier, M.; Cavelier, C. *Carcinogenesis* **1989**, *10*, 2043−2052.
(21) Heiple, J. M.; Taylor, D. L. In *Intracellular pH: Its Measurement, Regulation and Utilization in Cellular Functions*; Nuccitelli, R., Deamer, D. W., Eds.; Alan R. Liss, Inc.: New York, 1982; pp 21−54.
(22) Codd, R.; Lay, P. A.; Levina, A. *Inorg. Chem.* **1997**, *36*, 5440−5448.
(23) Codd, R.; Lay, P. A. *J. Am. Chem. Soc.* **1999**, *121*, 7864−7876.
(24) Irwin, J. A.; Hanson, G.; Lay, P. A. To be submitted for publication.
(25) Krumpolc, M.; Roček, J. *J. Am. Chem. Soc.* **1979**, *101*, 3206−3209.
(26) Judd, R. J.; Hambley, T. W.; Lay, P. A. *J. Chem. Soc., Dalton Trans.* **1989**, 2205−2210.
(27) Zhang, L.; Lay, P. A. *J. Am. Chem. Soc.* **1996**, *118*, 12624−12637.
(28) Goodgame, D. M. L.; Hayman, P. B.; Hathway, D. E. *Inorg. Chim. Acta* **1984**, *91*, 113−115.
(29) Boyko, S. L.; Goodgame, D. M. L. *Inorg. Chim. Acta* **1986**, *123*, 189−191.
(30) O'Brien, P.; Barrett, J.; Swanson, F. *Inorg. Chim. Acta* **1985**, *108*, L19−L20.
(31) Solids containing Cr(V) were isolated from the reactions of Cr(VI) with glutathione (O'Brien, P.; Pratt, J.; Swanson, F. J.; Thornton, P.; Wang, G. *Inorg. Chim. Acta* **1990**, *169*, 265−269) or ascorbate (Zhang, L. Ph.D. Thesis, University of Sydney, 1998); however, the structures of these Cr(V) compounds are still unclear.
(32) Quinic acid is widely distributed among higher plants, and its crystal structure has been determined (Abell, A.; Allen, F. H.; Bugg, T. D. H.; Doyle, M. J.; Raithby, P. R. *Acta Crystallogr., Sect. C* **1988**, *C44*, 1287−1290).
(33) Bkouche-Waksman, I. *Acta Crystallogr., Sect. C* **1994**, *C50*, 62−64.
(34) Codd, R.; Hambley, T. W.; Lay, P. A. *Inorg. Chem.* **1995**, *34*, 877−882.
(35) Bertagnolli, H.; Ertel, T. S. *Angew. Chem., Int. Ed. Engl.* **1994**, *33*, 45−66.
(36) Sakane, H.; Muñoz-Páez, A.; Díaz-Moreno, S.; Martínez, J. M.; Pappalardo, R. R.; Sánchez, M. E. *J. Am. Chem. Soc.* **1998**, *120*, 10397−10401.
(37) (a) Rich, A. M.; Armstrong, R. S.; Ellis, P. J.; Freeman, H. C.; Lay, P. A. *Inorg. Chem.* **1998**, *37*, 5743−5753. (b) Rich, A. M.; Armstrong, R. S.; Ellis, P. J.; Lay, P. A. *J. Am. Chem. Soc.* **1998**, *120*, 10827−10836.

Table 1. Spectroscopic and Stability Data for **Ia** in Solutions[a]

param	DMF	DMSO	H_2O (pH = 4.0)
UV-vis abs: λ, nm (ϵ, M^{-1} cm^{-1})	435 sh (637), 557 (206), 720 sh (49)	435 sh (662), 554 (248), 720 sh (60)	*b*
CD abs: λ, nm ($\Delta\epsilon$, deg M^{-1} m^{-1})	435 (+8.3), 540 (−19.3)	437 (+9.8), 553 (−26.9)	*b*
half-life[c]	14 days	11 days	10 min[d]
Cr(V) decomposed by disproportionation (eq 1), %[e]	10	30	90
EPR spectroscopy			
g_{iso} (species 1)[f]	1.9789	1.9787	1.9791
g_{iso} (species 2)	1.9783	1.9783	1.9787
10^4A_{iso}, cm^{-1} (species 1)[g]	16.5	16.5	16.4
10^4A_{iso}, cm^{-1} (species 2)	17.0	16.9	17.2
species 1, %[f]	70	80	45

[a] Spectra were taken at ~3 min after mixing of solid **Ia** with the corresponding solvent at 22 °C; [**Ia**] = 1.0 mM; no excess ligand was added. [b] Could not be determined due to significant decomposition of **Ia** during the dissolution. [c] Determined from the decrease of absorbance at 550 nm; the solutions were kept at 25 ± 1 °C and were protected from light. [d] This is an approximate value, since a significant portion of the amount of Cr(V) initially present decomposed before the measurement could be commenced. [e] Determined from the amount of formed Cr(VI)[22] at 60 days (for DMF or DMSO) or at 60 min (for H_2O) after the mixing. [f] Determined by simulation of the main EPR signal (due to $^{52}Cr + {}^{54}Cr$). [g] Hyperfine splitting due to ^{53}Cr (9.5 at. %); second-order corrections were applied in the calculations.

min^{-1}, capillary temperature 200 °C, *m*/*z* range 100−1000. Simulations of the ESMS spectra were performed using Masslynx software.[38] The FTIR spectra were acquired in a KBr matrix using the diffuse reflectance technique on a BioRad FTS-40 spectrometer. A Hewlett-Packard 8452 A diode-array spectrophotometer (λ = 300−800 nm; resolution, 2 nm; integration time, 0.2 s) was used for acquisition of the UV−visible spectra and for the measurements of the decomposition rates of **Ia**. A Jasco-710 spectropolarimeter (λ = 300−700 nm, resolution, 1 nm; scan rate, 500 nm/min; time constant, 0.125 s) was used for collection of the CD spectra. Magnetic susceptibility was measured on a Sherwood Scientific magnetic susceptibility balance. The balance was calibrated with $(NH_4)_2Fe(SO_4)_2 \cdot 6H_2O$, and diamagnetic corrections for the constituent atoms were calculated from the literature.[39] X-band EPR spectra were recorded using a quartz capillary (for the solids) or a flat quartz cell (for the solutions) on a Bruker EMX spectrometer equipped with a Bruker EMX 035M NMR gaussmeter and a Bruker EMX048T microwave frequency counter. The instrument settings were the following: center field, 3500 G; sweep width, 200 G; resolution, 1024 points; microwave frequency, ~9.66 GHz; microwave power, 2.0 mW; modulation frequency, 100 kHz, modulation amplitude, 0.97 G; time constant, 0.64 ms; sweep time, 5.24 s; number of scans, 5. Low-temperature EPR measurements were performed with a liquid-He-flow cryostat using a Bruker ER 4111 variable-temperature unit. The EPR spectra were processed using WIN-EPR software,[40] and simulations were performed using WinSim software.[41] Second-order corrections were applied in determining the EPR parameters from the spectra.

X-ray Absorption Spectroscopy and Data Processing. Chromium K-edge spectra of **Ia,b**[42] were recorded on the Australian National Beamline Facility (beamline 20B) at the Photon Factory, Tsukuba, Japan. The beam energy was 2.5 GeV, and the beam current, 280−360 mA. A Si[111] double-crystal monochromator was detuned by 50%. The spectra were recorded in transmission mode, using standard N_2-filled ionization chambers. Powder samples of **Ia** or **Ib** were mixed with BN (mass ratio **I**:BN = 2:1) and pressed into 0.5-mm pellets supported in an Al spacer between two 63.5-μm Kapton tape windows. The sample temperature for **Ia** was maintained at 14 ± 1 K using a closed-cycle He CryoIndustries REF-1577-D22 cryostat, while the data for **Ib** were collected at room temperature (~293 K). The low temperature used for data collection from **Ia** minimized its photodamage, improved the signal-to-noise ratio, and maximized the MS contributions to the XAFS spectrum.[37] The spectra were averaged from three (for **Ia**) or two (for **Ib**) scans taken at different positions on the sample and the edge energies differed by < 0.1 eV between the scans. The energy scale was calibrated using a Cr foil as an internal standard (calibration energy, 5989 eV, corresponded to the first peak of the first derivative of Cr(0) edge). Averaging, background subtraction, and the calculation of theoretical XAFS spectra were performed using the *XFIT* software package,[43] including FEFF 4.06[44] and FEFF 6.01[45] algorithms (for SS and MS, respectively), as described previously.[37] Overdeterminancy of the models used for XAFS calculations was checked by the method of Binsted et al.,[46] taking into account the applied restraints. The random errors in the estimated XAFS parameters, arising from the noise in the data, were determined by Monte Carlo analysis within the *XFIT* software.[43]

Molecular Mechanical Calculations. Model structures for the XAFS analysis were produced using MOMEC[47] software. The force fields were developed[48] using both published[49,50] force constants and those estimated from the IR data.[48] Starting coordinate sets were obtained from the X-ray crystal structures of **II**,[26] qaH_5,[32] and $(NH_4)_2\{[V^V(O)_2]_2[V^{IV}(O)](\mu\text{-}qaH_2)_2\} \cdot H_2O$.[34]

Results

Formation of a Cr(IV) Intermediate during the Synthesis of Ia. Complex **Ia** was isolated from the reaction of $K_2Cr_2O_7$ with excess qaH_5 in methanol.[23] This solvent was chosen (in place of acetone used in the synthesis of **II**)[25] because of the higher solubility of qaH_5. Immediately after mixing of $K_2Cr_2O_7$ (1.40 mmol) with qaH_5 (8.37 mmol) in methanol (500 mL) (optimal conditions for the synthesis of **Ia**),[23] the reaction solution turned pink, suggesting the formation of a Cr(IV) intermediate.[22] After ~15 min, the reaction mixture became brown-red due to the formation of Cr(V)[25] (confirmed by EPR spectroscopy; see below). To establish the nature of the intermediate(s), the reaction was repeated at a lower [Cr] to

(38) *Masslynx 3.2;* Micromass Ltd.: Manchester, U.K., 1998.
(39) Mabbs, F. E.; Machin, D. J. *Magnetism and Transition Metal Complexes*; Chapman and Hall: London, 1973.
(40) *WIN-EPR, Version 921201*; Bruker-Franzen Analytic: Bremen, Germany, 1996.
(41) *WinSim. EPR Calculations for Windows. Version 0.96*; National Institute of Environmental Health Sciences: Research Triangle Park, NC, 1995.
(42) Since XAFS is specific to the absorbing element, coprecipitation of a ligand oxidation product with **Ib** will not compromise the quality of XAFS data nor affect the data analysis, if it does not coordinate to the metal ion.
(43) (a) Ellis, P. J.; Freeman, H. C. *J. Synchrotron Radiat.* **1995**, *2*, 190−195. (b) *XFIT for Windows'95;* Australian Synchrotron Research Program: Sydney, Australia, 1996.
(44) Mustre de Leon, J.; Rehr, J. J.; Zabinsky, S. I.; Albers, R. C. *Phys. Rev. B.* **1991**, *44*, 4146−4156.
(45) Rehr, J. J.; Albers, R. C.; Zabinsky, S. I. *Phys. Rev. Lett.* **1992**, *69*, 3397−3400.
(46) Binsted, N.; Strange, R. W.; Hasnain, S. S. *Biochemistry* **1992**, *31*, 12117−12125.
(47) Hambley, T. W. *MOMEC 87. Program for Strain-Energy Minimization*; University of Sydney: Sydney, Australia, 1987.
(48) Codd, R. Ph.D. Thesis. University of Sydney, 1998.
(49) Hambley, T. W. *Acta Crystallogr., Sect. B* **1988**, *B44*, 601−609.
(50) Brubaker, G. R.; Johnson, D. W. *Coord. Chem. Rev.* **1984**, *53*, 1−36 and references therein.

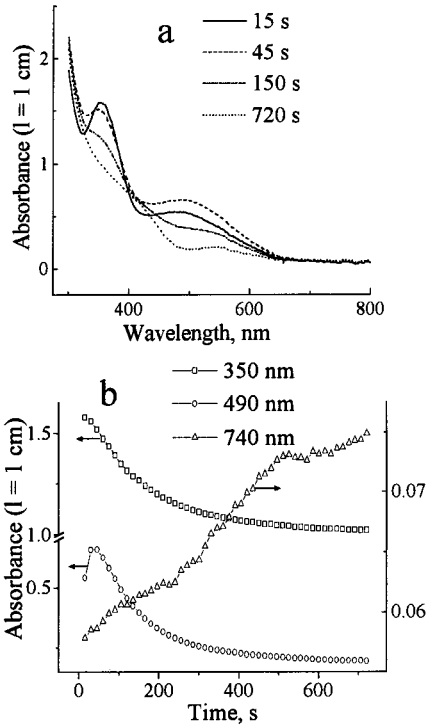

Figure 1. Typical UV−visible spectral changes (a) and characteristic kinetic curves (b) for the reaction of 1.0 mM Cr(VI) ($K_2Cr_2O_7$) with 20 mM qaH_5 in MeOH at 25 °C.

produce a homogeneous solution (1.0 mM Cr(VI) + 20 mM qaH_5 in MeOH, 25 °C); the observed UV−visible absorbance changes are shown in Figure 1. The absorbance at $\lambda_{max} = 490$ nm, characteristic of a Cr(IV) quinato complex,[22] increased during the first ∼45 s of the reaction and then decreased over ∼15 min with the formation of a shoulder at $\lambda = 500-600$ nm, characteristic of Cr(V) 2-hydroxycarboxylato complexes (Figure 1a).[2,25] Simultaneously, the absorbance due to Cr(VI) with $\lambda_{max} = 350$ nm decreased, and a weak absorbance at 700−750 nm, which is specific for Cr(V) complexes,[2] increased (Figure 1a,b).

To assess the roles of ligand and solvent in the formation of Cr(IV), the reactions of 1.0 mM Cr(VI) with 20 mM Lig (where Cr(VI) = $K_2Cr_2O_7$; Lig = $ehbaH_2$ or qaH_5) were performed in methanol, ethanol, 2-propanol, *tert*-butyl alcohol, acetone, DMF, or DMSO. The transient absorbances of the Cr(IV) intermediates (λ_{max} = 512 nm for Cr(IV)−ehbaH or 490 nm for Cr(IV)−qaH_4)[22] were observed only in the first three solvents.

Electrospray Mass Spectroscopy. Typical mass spectra of **Ia** are shown in Figure 2. The only significant (≥1%) signal in the negative-ion mode for a solution of **Ia** in DMF (∼1 mM) was that with m/z = 448.7 (Figure 2a) and an isotopic distribution corresponding to a $C_{14}H_{20}O_{13}Cr(1-)$ species (observed and simulated distributions are shown in Figure 2c,d). These results, together with the microanalytical data, allowed the assignment of the molecular formula of **Ia** as $K[Cr^{V}O(qaH_3)_2]\cdot H_2O$. A solution of **Ia** in H_2O/MeOH (50% volume MeOH; [**Ia**] ∼ 1 mM; pH = 4.0; time after mixing ∼1 min at 22 °C) showed, in addition to the signal at m/z = 448.7 (relative abundance 100%), a significant signal with m/z = 191.2 (12%), corresponding to qaH_4^- (Figure 2b). This suggests a fast decomposition of **Ia** in aqueous solution.[51] Solutions of **Ia** in either DMF or H_2O/MeOH did not show any significant signals in the positive-ion mode.

Vibrational Spectroscopy. The FTIR spectra of **Ia** and the free ligand (qaH_5) are shown in Figure S1 (Supporting Information) together with the corresponding spectra of **II** and $ehbaH_2$. The following features are characteristic for the spectrum of **Ia** in comparison with qaH_5: (i) the appearance of a strong band due to Cr═O stretching mode at 993 cm^{-1};[2] (ii) the disappearance of bands due to O−H (carboxyl) stretches at 2200−3000 cm^{-1}; (iii) the broadening of bands due to O−H (alcohol) groups at 3200−3500 cm^{-1} (these strong bands, which are present both in **Ia** and qaH_5 but absent in $ehbaH_2$ (Figure S1), are assigned to the 3,4,5-OH groups of quinato ligand); (iv) the broadening of the C═O stretching band at ∼1680 cm^{-1}. In the FTIR spectrum of **Ib** (see Experimental Section), multiple (>10) sharp peaks due to C═O stretches were observed between 1700 and 1630 cm^{-1}. This is in agreement with the microanalytical data, suggesting the coprecipitation with a ligand oxidation product.

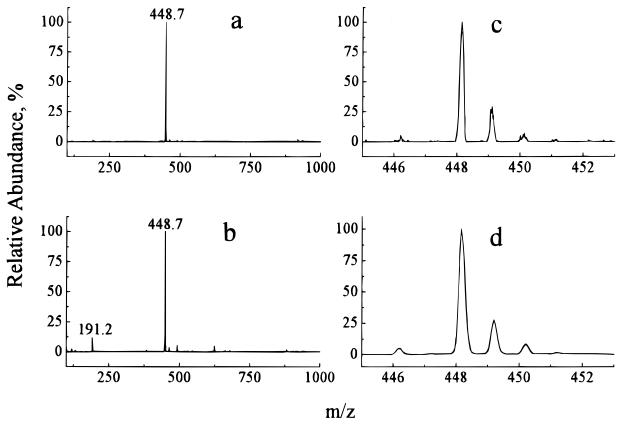

Figure 2. Typical ESMS (negative-ion mode) of ∼1 mM solutions of **Ia** in DMF (a) or H_2O/MeOH (1:1 v/v), pH = 4.0 (b) and experimental (c) and simulated for $C_{14}H_{20}O_{13}Cr(1-)$ (d) isotopic distribution of the main signal. The spectra were taken within ∼1 min after mixing of solid **Ia** with the solvent at 22 °C.

Electronic Spectroscopy and Stability Studies. Typical UV−visible and CD spectra of **Ia** ([**Ia**] = 1.0 mM; time after mixing ∼3 min at 22 °C) in DMF, DMSO, and H_2O (pH = 4.0) are shown in Figure S2 (Supporting Information), and a summary of the spectral data is given in Table 1. The spectra show the relative stability of **Ia** in solutions of DMF and DMSO and its significant decomposition on dissolution in water. Half-lives ($t_{1/2}$) of solutions of **Ia** (1.0 mM) in these solvents (25 °C, in the absence of light), measured by UV−visible spectroscopy, are given in Table 1. Similar stabilization of Cr(V) in aprotic solvents was previously observed for **II**,[26] although the lifetimes were much longer.[52] Solid **Ia** kept for 1 year at ambient temperature (protected from light and moisture) did not show any significant decomposition (UV−visible and IR spectroscopies).

In solution, Cr(V) complexes decompose by parallel disproportionation (eq 1) and ligand oxidation (eq 2) reactions.[53] To

$$3Cr(V) \rightarrow 2Cr(VI) + Cr(III) \quad (1)$$

$$Cr(V)-Lig \rightarrow Cr(III) + \text{oxidized Lig} \quad (2)$$

establish the extent of each pathway in the decomposition of

(51) Minor signals in the ESMS of **Ia** in H_2O/MeOH (Figure 2b) were attributed to the Cr(III) products of the decomposition of **Ia** on the basis of their m/z values and isotopic distribution patterns: $[Cr^{III}(qaH_3)_2(MeOH)]^-$ (m/z = 462.5; relative abundance 3.5%); $[Cr^{III}(qaH_3)(qaH)(MeOH)_2]^-$ (m/z = 492.2; 5.5%; qaH = oxidized quinato(2−)); $[Cr^{III}(qaH_3)(qaH_4)_2]^-$ (m/z = 624.3; 5.0%).

(52) Half-lives for solutions of **II** (1.0 mM) at 25 °C, measured by decrease of absorbance at 550 nm, were ∼2 h (H_2O, pH = 4) and >6 months (DMF or DMSO).

(53) Krumpolc, M.; Roček, J. *Inorg. Chem.* **1985**, *24*, 617−621.

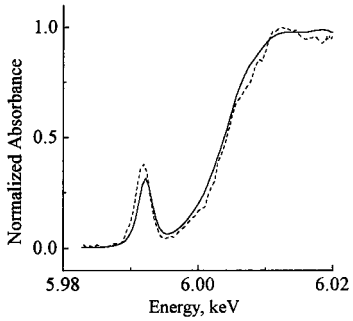

Figure 3. XANES spectra of solid **Ia** in BN (solid line) and of 10 mM solution of **II** in 1.0 M ehba buffer, pH 3.5 (dashed line, data of ref 57) at 14 K.

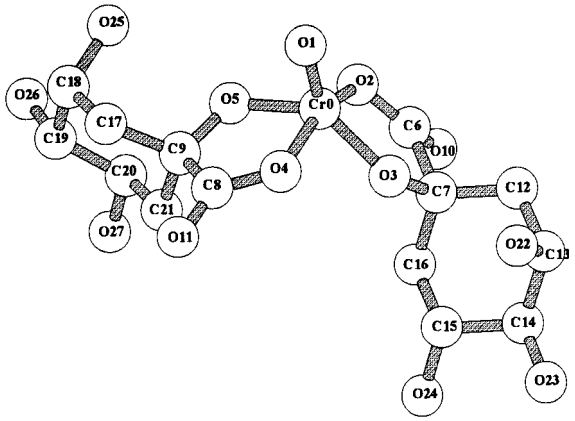

Figure 4. Structure of solid **Ia** (14 K) optimized by MS XAFS modeling (model 14, Table S5). Numbering of the atoms corresponds to those used in the XAFS calculations (Tables S3−S6).

Ia in different solvents, the reaction mixtures (at $t \sim 5t_{1/2}$) were diluted 10 times with 0.10 M NaOH and the absorbance of Cr(VI) was determined at 372 nm.[22] The results (Table 1) show that the fast decomposition of **Ia** in H_2O occurs mainly by disproportionation, while ligand oxidation (and/or solvent oxidation) dominates in the slow decompositions of **Ia** in DMF or DMSO.

Magnetic Moment and EPR Spectroscopy. The room temperature (∼293 K) magnetic moment of **Ia** ($\mu_{eff} = 2.10\ \mu_B$) is consistent with the presence of a single unpaired electron as expected for the Cr(V) oxidation state (d^1). The magnetic moment is slightly higher than the spin-only value but similar to those of Cr(V) complexes with 2-hydroxycarboxylato ligands, ehba, and hmba ($2.05\ \mu_B$).[2] Solid-state EPR spectra of **Ia** (Figure S3 in Supporting Information) were similar at both 298 and 14 K and consisted of a single broad signal with $g = 1.979$. Under similar conditions, the EPR signals of **II** possessed the same g value, but the line widths were 2−3 times smaller than those for **Ia** (Figure S3). The solution EPR spectrum from the reaction of Cr(VI) (1.0 mM) with qaH_5 (20 mM) in methanol (reaction time 15 min at 22 °C; Figure S4 in Supporting Information) showed a main signal ($g_{iso} = 1.9785$; $A_{iso}(^{53}Cr) = 17.0 \times 10^{-4}$ cm^{-1}), resembling that of the solution EPR spectra of **II**.[3] As for the latter, the outer ^{53}Cr satellite signals for Cr(V) in the reaction mixture are split (Figure S4), suggesting the presence of at least two geometric isomers.[2,23,54] The solution EPR spectra of **Ia** (1.0 mM) in DMF, DMSO, or H_2O (Figure S5 in Supporting Information) show the splitting of both the central peak and ^{53}Cr satellites; g_{iso} values and the ratio of signals are solvent-dependent (Table 1). Detailed studies of the EPR spectra of **Ia** in solutions are reported elsewhere.[23]

X-ray Absorption Spectroscopy. The XANES spectrum of **Ia** (Figure 3) features an edge jump at 6004.5 eV and a moderately intense pre-edge peak due to the symmetry-forbidden 1s → 3d transition[55,56] at 5992 eV. The XANES spectrum of **Ia** is similar to that of **II** (Figure 3)[57] but significantly different from those of Cr(III), Cr(IV) or Cr(VI) complexes.[55−57]

From structural models of **Ia** tested by SS[44] and MS[45] fitting of the XAFS spectrum (Tables S1−S6 and Figures S6−S8 in Supporting Information), acceptable models were those possessing both low goodness-of-fit values ($R \leq 22\%$) and physically reasonable values of the fitting parameters: the threshold energy E_0, the scale factor S_0^2, and the Debye−Waller factors σ_i^2.[43] Restraints applied to the fitting parameters are given in Table S1, and the applied window functions are shown in Figure S6. In the SS modeling of the first coordination shell (Table S2), a very good fit ($R = 9.9\%$) was obtained for the model including one short (1.56 Å), two intermediate (1.81 Å), and two longer (1.92 Å) Cr−O bonds (model 1 in Table S2). These bond lengths are close to those for the oxo, alcoholato, and carboxylato ligands in **II** (1.547, 1.796, and 1.903 Å, respectively), found by X-ray crystallography.[26] Alternative models of **Ia**, including, in addition to the oxo ligand (∼1.55 Å), either four alcoholato ligands (∼1.80 Å) or three alcoholato (∼1.80 Å) and one carboxylato (∼1.90 Å) ligands, led to both poorer R values and significantly higher Debye−Waller factors σ_i^2 for the alcoholato or carboxylato O atoms (models 2 and 3 in Table S2). Models including longer Cr−O bonds (≥2.0 Å) improved the R values but gave unreasonably low values of σ_i^2 for these bonds (models 4 and 5 in Table S2). Notably, all the mentioned models gave significantly higher values of σ_i^2 for the oxo O atom than those usually found for the donor atoms of the first coordination shell (∼0.006 instead of 0.001−0.003).[37,43] Models that did not include short (∼1.55 Å) Cr−O bonds or included more than one of them gave very poor fits (models 6−9 in Table S2).

The results of SS modeling are consistent with other spectroscopic evidence that **Ia** exists in the solid state as an oxo complex with two quinato ligands bound in 2-hydroxycarboxylato fashion. This model was further refined by MS fitting, the results are presented in Tables S3−S6 and Figures S7 and S8. In all the applied MS models, Cr−O bond lengths were restrained close (±0.05 Å) to those found by SS calculations, and the bond lengths and angles involving C atoms of quinato ligands were restrained to correspond (±0.05 Å, ±5°) to their hybridization states (sp^2 for C6 and C8 and sp^3 for C7, C9, and C12−C21, Figure 4); the corresponding restraints are enumerated in Tables S3 and S5.

Initially, MS modeling included the first three coordination shells of **Ia** (atoms 0−12, 16, 17, and 21 in Figure 4, models 10−13 in Tables S3 and S4) and was started from two independent structures: (i) optimized MM model of **Ia**[48] (model 10a); (ii) X-ray crystal structure of **II**[26] (model 10b). Both optimizations led to identical values of bond lengths and Debye−Waller factors (Tables S3 and S4), but some optimized bond angles (especially those involving the oxo group of **Ia**) were significantly different for the both models (Table S3), despite the close R values (21.3% for 10a and 21.6% for 10b,

(54) Bramley, R.; Ji, J.-Y.; Judd, R. J.; Lay, P. A. *Inorg. Chem.* **1990**, *29*, 3089−3094.
(55) Bajt, S.; Clark, S. B.; Sutton, S. R.; Rivers, M. L.; Smith, J. V. *Anal. Chem.* **1993**, *65*, 1800−1804.
(56) Ellis, P. J.; Joyner, R. W.; Maschmeyer, T.; Masters, A. F.; Niles, D. A.; Smith, A. K. *J. Mol. Catal. A* **1996**, *111*, 297−305.
(57) Levina, A.; Foran, G. J.; Lay, P. A. *J. Chem. Soc., Chem. Commun.* **1999**, 2339−2340.

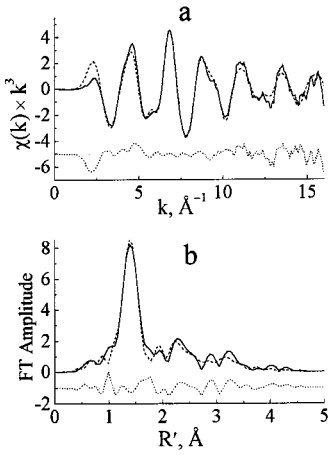

Figure 5. Application of the MS model, corresponding to Figure 4 to the XAFS spectrum (a) and its FT (b) of the solid **Ia** (14 K). Solid lines are the windowed observed spectra, dashed lines are the windowed calculated spectra, and dotted lines are the fit residues. The optimized XAFS parameters are enumerated in Table S5, and the applied window function is shown in Figure S6d.

Figure S7). Further MS fittings (models 11−13, Tables S3 and S4) were performed starting from the optimized model 10a.

The Cr−O bond lengths, determined from the models 10a,b (1.57, 1.82, and 1.94 Å) are longer than the corresponding values in the crystal structure of **II** (see above), but the differences (0.02−0.04 Å) are close to the expected systematic errors of XAFS calculations.[36] To check whether the differences in bond lengths between **Ia** and **II** were significant, model 11 was applied, where the values of Cr−O bond lengths were tightly (±0.01 Å) restrained to those of **II**. This led to significant deterioration of the fit (R = 29.9%, Figure S8). Thus, the increase in Cr−O bond lengths in **Ia** in comparison with **II** is significant.

In models 10 and 11, bond angles between the ligands were allowed to change freely during the optimization. In model 12, the bond angles between quinato ligands were restrained close (±5°) to those in the crystal structure of **II**. The optimized fit was only slightly worse (R = 22.0%, Figure S8) than that of model 10a. However, deterioration of the fit was more significant for model 13 (R = 25.3%, Figure S8), where the angles between oxo and quinato ligands were restrained. Thus, while reproducible values of bond angles involving the oxo group of **Ia** could not be obtained from the MS calculations (models 10a,b, Table S3), these angles are likely to differ significantly from the corresponding angles in **II**.

The MS XAFS fit was then expanded to include all non-H atoms in the proposed structure of **Ia** (model 14, Table S5), using the initial coordinates of the optimized MM model of **I**.[48] Inclusion of the more distant coordination shells to model 14 did not improve the fit (Figure 5, R = 21.3%) compared to model 10a (Figure S7, R = 21.3%). Initial calculations of model 14 used a maximum effective path length value r_{max} = 5.0 Å and the maximum number of MS legs N = 5. Repeated calculations with N = 4 or r_{max} = 5.5 Å did not change the fit significantly. The most significant scattering paths with N = 2−5 for model 14 are enumerated in Table S6. The results of the best SS and MS XAFS fits for **Ia** are summarized in Table 2.

The results of SS XAFS fittings for **Ib**, including the first three coordination shells, are summarized in Table S7, Supporting Information. Consistent with the analysis for **Ia**, the best fit of the first coordination shell corresponded to one oxo, two alcoholato, and two carboxylato O atoms with the Cr−O bond lengths 1.58, 1.83, and 1.96 Å, respectively (Table 2). Application of alternative models, including, in addition to the oxo group, either three alcoholato and one carboxylato donors or four alcoholato donors, led to deterioration of the fits and/or to unreasonable σ_i^2 and S_0^2 values (Table S7). All applied models gave unusually high σ_i^2 values for an oxo O atom (Tables 2 and S7). Several attempts were made to perform MS XAFS analysis for **Ib** using models generated by MM calculations; however, these did not refine well to a single three-dimensional structure and gave large R values.

Table 2. Summary of XAFS Modeling Results for **I**[a]

param[b]	SS (**Ia**)	SS (**Ib**)	MS (**Ia**)	MS (**Ia**)
atoms included (Figure 4)	0−5	0−12, 16, 17, 21	0−12, 16, 17, 21	0−27
XAFS window, Å^{-1} [c]	1−16	1−16	0−16	0−16
FT window, Å[c]	0.8−1.9	0.5−3.0	0−4	0−5
N_i/p[d]	1.3	1.5	1.2	1.1
R, %	9.9	15.3	21.3	21.3
ΔE_0, eV	−10.4	−7.2	−5.8	−4.1
S_0^2	0.89	0.98	0.89	0.89
O(oxo)				
X, Å	1.56	1.58	1.57	1.57
σ^2, Å^2	0.0057	0.0088	0.0084	0.0082
O(carboxylato)				
X, Å	1.92	1.96	1.94	1.94
σ^2, Å^2	0.0033	0.0016	0.0020	0.0019
O(alcoholato)				
X, Å	1.81	1.83	1.82	1.82
σ^2, Å^2	0.0024	0.0028	0.0012	0.0012

[a] Random errors arising from the noise in the data, estimated by Monte-Carlo method,[43] were ≤ 0.1 eV for ΔE_0, ≤ 0.01 for S_0^2, ≤ 0.002 Å for the bond lengths, and ≤ 2.0 × 10^{-4} Å^2 for σ_i^2; expected systematic errors for the bond lengths are 0.01−0.02 Å.[3] [b] Designations: R is the goodness-of-fit parameter;[43] $\Delta E_0 = E_0 - 6005$ eV, where E_0 is the threshold energy; S_0^2 is a scale factor; X values are the Cr−O distances; σ^2 values are the Debye−Waller factors. [c] Window functions are shown in Figure S6, Supporting Information. [d] Determinancy of the fit (N_i is the number of independent observations, and p is the number of varied parameters);[46] for $N_i/p > 1$, calculations are overdetermined and the results are valid.

In summary, the XAFS calculations have shown the following: (i) The bis(2-hydroxycarboxylato) binding mode of the quinato ligands to Cr(V) is most likely for the solid states of **Ia,b**, with the Cr−O bonds of the oxo, carboxylato, and alcoholato moieties in **I** being 0.02−0.05 Å longer than the corresponding bonds in **II**. (ii) The position of an oxo O atom in **Ia,b** is somewhat disordered, which is reflected in high Debye−Waller factor values. (iii) The bond angles in **Ia**, involving the oxo group, are likely to differ significantly from those in **II**.

Discussion

Proposed Mechanism of the Formation of I. The first step in the proposed mechanism (eq 3 in Scheme 1) is the two-electron reduction of Cr(VI) by methanol (or other primary or secondary alcohol solvents), leading to Cr(IV) (probably via the formation of chromate esters).[58] Although a similar reaction with the participation of the secondary OH groups of qaH_5 is not excluded, methanol is likely to play a major role in the reaction (eq 3), as the formation of a Cr(IV)−ehba complex was observed during the Cr(VI) + $ehbaH_2$ reaction in this solvent (unlike qaH_5, $ehbaH_2$ does not have easily oxidizible alcohol moieties). In the following fast step (eq 4 in Scheme

(58) Mitewa, M.; Bontchev, P. R. *Coord. Chem. Rev.* **1985**, *61*, 241−272 and references therein.

Scheme 1. Proposed Mechanism for the Formation of **I** during the Reaction of $[Cr_2O_7]^{2-}$ with Excess qaH_5 in Methanol

$$[\overset{VI}{Cr_2O_7}]^{2-} + CH_3OH \xrightarrow{slow} [\overset{VI}{CrO_4}]^{2-} + H_2\overset{IV}{CrO_3} + HCOH \quad (3)$$

$$H_2\overset{IV}{CrO_3} + 2\,qaH_5 \overset{fast}{\rightleftharpoons} [\overset{IV}{CrO}(qaH_4)_2]^0 + 2\,H_2O \quad (4)$$

$$[\overset{IV}{CrO}(qaH_4)_2]^0 + RCH_2OH \xrightarrow{slow} Cr(III) + R\dot{C}HOH \quad (5)$$

$$[\overset{VI}{CrO_4}]^{2-} + R\dot{C}HOH \xrightarrow{fast} [H\overset{V}{CrO_4}]^{2-} + RCOH \quad (6)$$

$$[H\overset{V}{CrO_4}]^{2-} + 2\,qaH_5 \overset{fast}{\rightleftharpoons} [\overset{V}{CrO}(qaH_3)_2]^- + 2\,H_2O + OH^- \quad (7)$$

$$[\overset{IV}{CrO}(qaH_4)_2]^0 + [\overset{VI}{CrO_4}]^{2-} + H_2O \xrightarrow{slow} 2\,[\overset{V}{CrO}(qaH_3)(OH)_2]^- \quad (8)$$

$$[\overset{V}{CrO}(qaH_3)(OH)_2]^- + qaH_5 \overset{fast}{\rightleftharpoons} [\overset{V}{CrO}(qaH_3)_2]^- + 2\,H_2O \quad (9)$$

1), Cr(IV) is stabilized by complexation with qaH_5, probably via the protonated 2-hydroxycarboxylato moieties.[22] A possible mechanism for the formation of Cr(V) (eqs 5−7 in Scheme 1) is similar to that proposed for the reaction of Cr(VI) with oxalic acid in acidic aqueous media[59] and involves the one-electron reduction of Cr(IV) by methanol or qaH_5 (eq 5) and then a fast reaction of the resultant organic radical with Cr(VI) (eq 6), followed by stabilization of the formed Cr(V) by the ligand (eq 7). Another possible mechanism for the formation of **I** involves the comproportionation of Cr(IV) and Cr(VI) (eq 8 in Scheme 1).[60] The equilibrium between **I** and the corresponding monochelate (eq 9 in Scheme 1) is similar to that observed experimentally for **II** in alcohol solutions.[54] Both alternatives (eqs 5−7 and 8 and 9) are in agreement with the observed similarity in decay rates of Cr(IV) and Cr(VI) (Figure 1). Further studies of the redox properties of Cr(IV) quinato complexes are required to distinguish between these mechanisms.

Evidence for the Bis[2-hydroxycarboxylato(2−)] Binding Mode in I. Either 2-hydroxycarboxylato or 1,2-diolato ligands of qaH_5 are capable of stabilizing Cr(V).[23,24,59,61] Modeling of the first coordination shell of **Ia,b** using SS shows a significant preference for the bis[2-hydroxycarboxylato(2−)] model over the bis[1,2-alcoholato(2−)] or the mixed-ligand binding models. As the resolution in bond lengths for the SS analyses of the XAFS data with $k_{max} = 16$ Å^{-1} is ∼0.1 Å,[62] Cr−O bonds with lengths of ∼1.90 Å (carboxylato) and ∼1.80 Å (alcoholato)[26] cannot be distinguished with certainty from the SS data alone. The values of bond lengths were confirmed by the results of MS XAFS analysis for **Ia**. The optimized values of Cr−O bond lengths (Tables 2 and S3) were independent, within the experimental error (0.02 Å),[37] on the nature of counterion in **I** (K^+ or Na^+) and on the calculation method (SS or MS), as well as on the initial model used for MS calculations. However, no unique three-dimensional structure of **I** could be found by MS XAFS calculations (compare models 10a, 10b, and 14 in Tables S3 and S5). This feature may reflect the presence of several geometric isomers with close energies in the solid states of **Ia,b**.[23,54] While the *R* factors for the fits are around 20%, most of those reside in the atomic region of the XAFS ($k < 3$, Figure 5), which are often not modeled well,[37,43] so the fits to the structures are somewhat better than indicated by the *R* values.

If complex **I** contains two 1,2-diolato donors or one diolato and one 2-hydroxycarboxylato donor, the resulting species in solutions are expected to possess a charge of 3− or 2−, respectively, due to deprotonation of the free carboxyl group. However, the absence of significant amounts (≥5%) of such species in solutions of **Ia** in DMF, DMSO, or H_2O/MeOH (pH = 4.0) was established by ESMS (Figure 2). Participation of both the 2-hydroxycarboxylato moiety and the secondary OH groups of qaH_5 in the complexation is likely to lead to the formation of polynuclear complexes.[23,33,34] However, ESMS did not reveal any significant amounts of such species in the solutions of **Ia** (Figure 2).

The proposed structure of **Ia** is also consistent with the loss of the bands due to carboxylic acid O−H stretching modes at 2200−3000 cm^{-1} and the g_{iso} values in the solution EPR spectra of **I** (1.9780−1.9790),[3] since significantly higher g_{iso} values (∼1.9800) are characteristic for Cr(V) 1,2-diolato complexes.[3,23,24,61] Finally, the UV−visible and XANES spectra of **Ia** (Table 1, Figures 3 and S2) are remarkably similar to those of **II**.[25,57]

All the evidence outlined shows that **I** exists predominantly (>95%) as a bis[2-hydroxycarboxylato(2−)] complex under the conditions used in this work (both in solid state and in solutions). Indeed, the detailed EPR spectroscopic studies of the speciation of **Ia** in solutions[23] have shown that the linkage isomers of **I** involving the 1,2-diolato moieties of the quinato ligands only appear in substantial amounts relative to the bis(2-hydroxycarboxylato) isomers in water at pH ≥ 6.

Hydrogen Bonding in I. Hydrogen bonding involving the 3,4,5-OH groups of the quinato ligands, the oxo O atoms, and possibly the carbonyl O atoms in the solid state of **I** is evident from the following: (i) high values of Debye−Waller factors for the oxo O atom in all of the XAFS models (Tables 2, S2, S4, S5, and S7) and a difference in bond angles involving the oxo group in **Ia** and **II**, found by MS XAFS; (ii) broadening of the solid-state EPR signals of **Ia** in comparison with **II** (Figure S3); (iii) broadening of the signals due to 3,4,5-OH and carboxyl C═O groups in the IR spectrum of **Ia** (Figure S1). Similar inter- and intramolecular hydrogen bonds were found in the crystal structure of the mixed-valence V(IV/V) quinato trimer.[34]

Structure and Solution Stability of I. Formation of intermolecular hydrogen bonds in the solutions of **I** may facilitate the disproportionation reaction (eq 1). Elongation of the Cr−O bonds in **I** compared to **II** (Table 2), which is probably caused by the bulky nature of the quinato ligands, can also contribute to the much shorter lifetimes of solutions of **I** in comparison with those of **II** (Table 1).[52]

Biological Relevance of I. Compound **Ia** is the first isolated[23] and fully characterized Cr(V) complex with a naturally occurring, optically active ligand.[31] The pH-dependent equilibria between 2-hydroxycarboxylato and diolato Cr(V) species are thought to mimic those of Cr(V) in intracellular media, which is directly related to Cr-induced carcinogenesis.[2,3,23,24] Synthesis of **Ia** led to the ability to perform intramolecular competition experiments on the relative thermodynamic stabilities of these two biologically relevant binding modes to Cr(V) under different pH conditions.[23] Finally, the ability of **Ia** to cleave DNA under biologically relevant conditions has been recently shown.[11]

Acknowledgment. Financial support of this work by an Australian Research Council (ARC) grant (to P.A.L.), Australian Postgraduate Research Scholarship (to R.C.), AusAID Ph.D. Scholarship (to L.Z.), and ARC RIEFP grants for EPR, CD,

(59) Farrell, R. P.; Lay, P. A.; Levina, A.; Maxwell, I. A.; Bramley, R.; Brumby, S.; Ji, J.-Y. *Inorg. Chem.* **1998**, *37*, 3159−3166.
(60) Gould, E. S. *Coord. Chem. Rev.* **1994**, *135/136*, 651−684.
(61) Bramley, R.; Ji, J.-Y.; Lay, P. A. *Inorg. Chem.* **1991**, *30*, 1557−1564.
(62) Riggs-Gelasco, P. J.; Stemmler, T. L.; Penner-Hahn, J. E. *Coord. Chem. Rev.* **1995**, *144*, 245−286 and references therein.

and ESMS equipment and the 10-element Ge detector is gratefully acknowledged. X-ray absorption spectroscopy was performed at the Australian National Beamline Facility with support from the Australian Synchrotron Research Program, which is funded by the Commonwealth of Australia under the Major National Research Facilities program. The authors thank the Australian National University Microanalytical Service for the microanalyses, Professor Hans Freeman (University of Sydney), Drs. Garry Foran and James Hester (the Australian National Beamline Facility in Tsukuba), and Dr. Daniel Shi for assistance with the collection of the X-ray absorption spectra, Professor Freeman for helpful comments on the analysis and the manuscript, and Drs. Xiaomin Song and Sejin Jeong (University of Sydney) for assistance with the ESMS.

Supporting Information Available: Figures showing typical FTIR spectra of **Ia**, **II**, qaH_5, and $ehbaH_2$, typical UV−visible and CD spectra of **Ia** in solutions, typical solid-state and solution EPR spectra of **Ia**, window functions used in the analyses of the XAFS spectrum of **Ia**, and the results of different MS fits of the XAFS spectrum of **Ia** and tables listing the details of SS and MS XAFS calculations for **Ia,b**. This material is available free of charge via the Internet at http://pubs.acs.org.

IC990730B